Inorganic Chemistry

pubs.acs.org/IC

Article

Force-Activated Spin-Crossover in Fe^{2+} and Co^{2+} Transition Metal Mechanophores

Xiao Huang, Ilia Kevlishvili, Stephen L. Craig, and Heather J. Kulik*

Cite This: *Inorg. Chem.* 2025, 64, 380−392

Read Online

ACCESS | Metrics & More | Article Recommendations | Supporting Information

ABSTRACT: Transition metal mechanophores exhibiting force-activated spin-crossover are attractive design targets, yet large-scale discovery of them has not been pursued due in large part to the time-consuming nature of trial-and-error experiments. Instead, we leverage density functional theory (DFT) and external force explicitly included (EFEI) modeling to study a set of 395 feasible Fe^{2+} and Co^{2+} mechanophore candidates with tridentate ligands that we curate from the Cambridge Structural Database. Among nitrogen-coordinating low-spin complexes, we observe the prevalence of spin crossover at moderate force, and we identify 155 Fe^{2+} and Co^{2+} spin-crossover mechanophores and derive their threshold force for low-spin to high-spin transition (F_{SCO}). The calculations reveal strong correlations of F_{SCO} with spin-splitting energies and coordination bond lengths, facilitating rapid prediction of F_{SCO} using force-free DFT calculations. Then, among all Fe^{2+} and Co^{2+} spin-crossover mechanophores, we further identity 11 mechanophores that combine labile spin-crossover and good mechanical robustness that are thus predicted to be the most versatile for force-probing applications. We discover two classes of *mer*-symmetric complexes comprising specific heteroaromatic rings within extended π-conjugation that give rise to Fe^{2+} mechanophores with these characteristics. We expect the set of spin-crossover mechanophores, the design principles, and the computational approach to be useful in guiding the high-throughput discovery of transition metal mechanophores with diverse functionalities and broad applications, including mechanically activated catalysis.

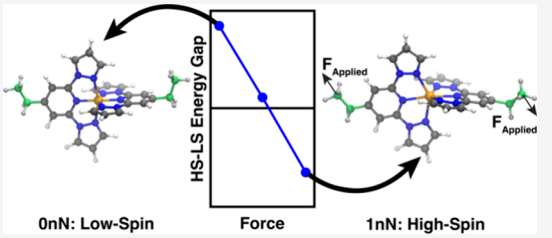

1. INTRODUCTION

Mechanophores are force-responsive molecular units that possess mechanically labile bonds[1−4] or otherwise change their properties (e.g., optical, magnetic) under force. Upon applied force, the bonds most commonly undergo controlled dissociation, rearrangement or elongation, and mechanophores consequently exhibit a wide range of responses including color change, i.e., mechanochromism,[5−7] luminescence,[8−10] small-molecule release,[11−14] and turn-on catalysis.[15,16] Consequently, mechanophores have been extensively studied in recent years as building blocks of responsive materials, and they have broad applications in fundamental reactivity studies,[17−19] force probing,[5−10] polymer strengthening,[20−23] drug and prodrug delivery,[11,12,24,25] and upcycling of waste polymers.[13,14,26,27] Although more than 100 mechanophores have been synthesized and studied, the majority of them are organic molecules.[4,28] Organic mechanophore force-probes rely on mechanochromism or turn-on emission responses, thus they are incompatible with most engineering polymers, which are translucent or opaque.[29,30] Additionally, only a few organic mechanophores with near-infrared emission thus compatible with *in vivo* biomedical sensing have been developed.[31,32]

Transition metal mechanophores have received growing attention as their mechanochemical activity can be readily altered by changing metal cations[33−36] or modifying ligand chemistry,[33,35,37] and they have been used as mechanochromic force probes,[33,37,38] mechanically activated catalysts,[15,16] metal-release agents,[39] and to strengthen polymer networks.[34,35,40] On the other hand, their potential application as spin-switchable force probes has remained less explored. Some low-spin (LS) Fe^{2+} complexes[41−44] and Co^{2+} complexes[45] have been identified to switch to high-spin (HS) under applied force as their coordination bonds are elongated and weakened. Most of the complexes are homoleptic, (bis)tridentate with terpyridine[41,45] or terpyridine derivative[42,43] ligands. These complexes exhibit mechanically activated turn-on magnetism, and they can thus be used as versatile force probes compatible with engineering polymers or biomedical implants.[46,47] The conductance changes accompanying LS-to-HS spin-crossover also make these complexes promising building blocks for molecular electronic devices.[41−45] Although a few complexes[41−45] and polymer−metal complex composites[48−50] exhibiting mechanically promoted spin-crossover have been reported, due to the complexity of experiments, no comprehensive mechanistic studies or large-scale screens have been conducted. Given the time-consuming nature of

Received: November 5, 2024
Revised: December 9, 2024
Accepted: December 12, 2024
Published: December 23, 2024

https://doi.org/10.1021/acs.inorgchem.4c04732
Inorg. Chem. 2025, 64, 380−392

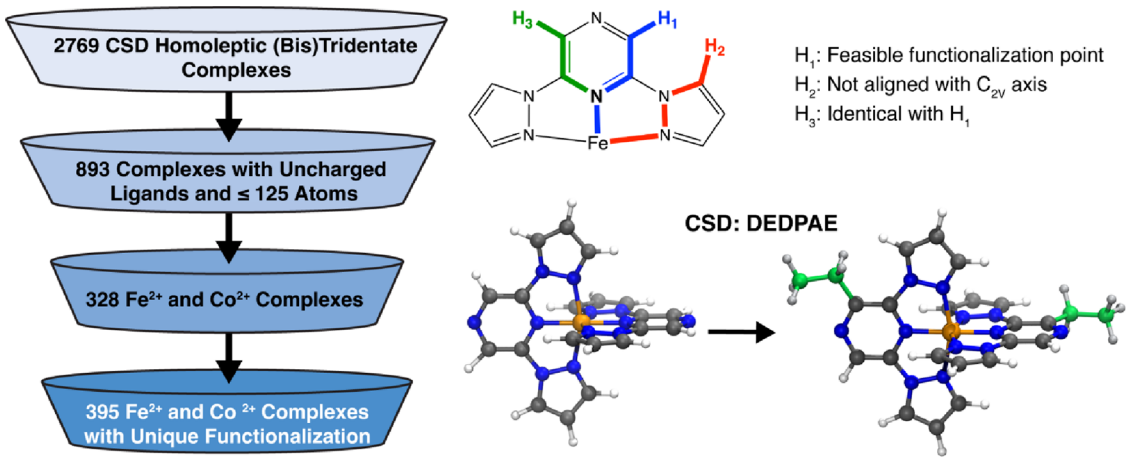

Figure 1. (Left) Workflow to repurpose CSD complexes as spin-crossover mechanophore candidates. (Right) Example of attachment point identification and functionalization of a *mer*-symmetric complex. Colors for atoms are as follows: orange for iron, gray for carbon, white for hydrogen, and blue for nitrogen. The carbon and hydrogen in functionalized ethyl groups used to mimic extended polymer strands are colored in light green and light gray for clarity.

experimental trial-and-error discovery of mechanophores, a computational approach is one alternative strategy for the larger-scale discovery of spin-crossover transition metal mechanophores.

Computational screening with density functional theory (DFT) has been leveraged to identify open-shell transition metal complexes exhibiting thermal spin-crossover[51−53] and catalytic activity.[54−57] To model the mechanical responses of bonds and molecules, such screening efforts must incorporate the effect of force in the simulation. One of the most straightforward techniques, the constrained geometries simulate external force (CoGEF) method, approximates a critical force by a series of successive constrained geometry optimizations.[58] Although CoGEF has been used for investigating various mechanophores and for computational screening of transition metal mechanophores,[7,59−61] the magnitude of external force is not explicitly defined, limiting its applicability to estimating the effect of force on spin state energetics. Alternatively, models defining force explicitly by incorporating an external potential term into DFT have been developed.[62] Among them, ab initio steered molecular dynamics (AISMD) methods[63] are versatile but require extensive statistics.[18,19,64−66] When an approximate minimum energy pathway is known, path-based search methods in the presence of applied force are a high-accuracy alternative. The force-modified transition state may be obtained with either the force-modified potential energy surface (FMPES) approach of Martínez and co-workers[63] or, equivalently, the external force explicitly included (EFEI) method of Marx and co-workers.[67] Both model the influence of external force on the potential energy surface, enabling the identification of force effects on spin state energetics and other molecular properties.[68−71] An additional concern arises from the accuracy of the underlying electronic structure model used in the force-applied simulations. Higher-cost methods such as double-hybrid DFT,[72] CASPT2,[73,74] CASPT2/CC,[75,76] and emerging multiconfigurational DFT methods[77,78] are expected to be more predictive than lower rungs of "Jacob's ladder" in DFT. Nevertheless, through parameter calibration[79−82] and selection of the optimal exchange-correlation functional,[83−85] the accuracy of standard global hybrid functional DFT in predicting LS−HS energy and structural differences of transition metal complexes can be improved.[86,87] It should be noted that a low-cost method is essential when paired with the numerous force-applied simulations required in a high-throughput screening scenario.

In this work, we carry out a large-scale screen of synthetically accessible Fe^{2+} and Co^{2+} complexes from the Cambridge Structural Database (CSD)[88] and curate a set of 395 complexes that are suitable for polymer network incorporation. With DFT and EFEI calculations, we demonstrate that force-activated spin-crossover is prevalent in LS Fe^{2+} and Co^{2+} complexes, and we identify 155 complexes as candidates for magnetic force probes and evaluate their spin-crossover critical force (F_{SCO}). To further accelerate computational screening, we develop methods to predict F_{SCO} of LS Fe^{2+} and Co^{2+} complexes that only rely on DFT, circumventing costly EFEI calculations. Among all force-probe candidates, we find 11 Fe^{2+} and Co^{2+} complexes with facile, reversible, and robust mechanochemical responses. Besides these complexes with facile spin-crossover and high dissociation force, we also discover a class of complexes with rapid dissociation of two coordination bonds to form square planar and potentially catalytically active complexes.

2. METHODS

2.1. Data Set Curation. We began by examining mononuclear, homoleptic, tridentate complexes in the Cambridge Structural Database (CSD),[88] version 5.41 (November 2019) combined with the March and May 2020 updates, to find transition metal complexes (TMCs) that are synthetically accessible and would be compatible with polymer network incorporation. We consider only homoleptic complexes as mechanophore candidates because it would be challenging to consistently assemble nonhomoleptic transition metal complex cross-linkers in polymers. We focused on (bis)tridentate complexes rather than (tris)bidentate complexes due to the greater simplicity of the dissociation events for tridentate complexes. From this set, we curated an initial set of 2,769 mononuclear, homoleptic, tridentate complexes comprising Mn, Fe, Co, Ni, Cu, Zn, and small numbers of other metals (Figure 1 and Supporting Information Figure S1). To ensure that the corresponding monomer would be relatively straightforward to synthesize and compatible with common polymerization reactions, we excluded complexes with ligands that had nonzero charge, as indicated by differences in the CSD-specified molecular charge and user-assigned metal oxidation state. We further eliminated complexes with greater than 125 atoms to avoid the high

https://doi.org/10.1021/acs.inorgchem.4c04732
Inorg. Chem. 2025, 64, 380−392

computational cost associated with modeling those complexes, yielding a set of 893 complexes of moderate size with neutral ligands (Figure 1). From these, we selected only Fe^{2+} and Co^{2+} complexes, which are among the most common metals in spin-crossover systems.[89−92] This leads to a final data set of 328 complexes. In terms of metal composition, the data set contains 222 Fe^{2+} and 106 Co^{2+} complexes. The candidates are predominantly *mer*-symmetric, with 259 *mer*-symmetric and 69 *fac*-symmetric complexes.

As shown in previous studies, higher force loading is required to activate mechanically labile bonds in a mechanophore if the force is propagated symmetrically along a mechanophore structure.[93−95] Therefore, to discourage ligand dissociation, we identified polymer attachment points (i.e., for attachment of ethyl groups that mimic polymer strands, see next) as hydrogen atoms that are most distant from the metal center, as measured by the shortest path length on a molecular graph. For *mer*-symmetric complexes, we further took inspiration from previous experimental studies and selected hydrogen atoms that are in proximity to the C_{2v} axis defined by the central coordination atom of each ligand.[33,34,96] Consequently, we required that the shortest path on molecular graph (or one of multiple shortest paths) connecting the attachment point and the metal center must pass through the middle coordination atom (Figure 1).

We successfully identified a single attachment point on each ligand and functionalized it with an ethyl group for 137 Fe^{2+} and 67 Co^{2+} complexes. For the remaining complexes, we found multiple potential hydrogen atoms equidistant from the metal center on each ligand. To analyze these potential attachment points systematically, we characterized the chemical environment of each hydrogen atom by replacing it with a chlorine atom and calculated the graph determinant of the resulting modified ligand. We consider two hydrogens on a ligand to be chemically equivalent if substituting either hydrogen results in modified ligands that have the same graph determinant. For 59 Fe^{2+} and 29 Co^{2+} complexes, this analysis revealed that multiple structures were chemically equivalent, and one structure was randomly selected from the duplicates (Figure 1). For 26 Fe^{2+} and 10 Co^{2+} complexes, multiple possible attachment points that are chemically nonequivalent were identified on each ligand (Supporting Information Figure S2). For these complexes, we matched hydrogen atoms with identical chemical environments on both ligands, modified them into ethyl groups, and treated each resulting structure as a separate candidate for simulation. This process yielded a set of 395 candidates, comprising 263 complexes Fe^{2+} and 132 Co^{2+} complexes. Among them, 295 complexes exhibited *mer* symmetry and 100 exhibited *fac* symmetry.

2.2. Computational Details. All electronic structure calculations were all performed using hybrid DFT in the gas phase using Orca v 5.0.1.[97,98] These calculations included gas-phase geometry optimizations and EFEI simulations as well as DFT functional benchmarking. Throughout all calculations, the def2-TZVP basis set was employed for transition metals and the def2-SVP basis set was used for all other atoms.[99] All calculations were carried out in the unrestricted formalism. The modified B3LYP functional[100−102] with the empirical D3 dispersion correction[103] using Becke−Johnson damping[104] was employed. The modified functionals were defined as the following:

$$E^{\mathrm{B3LYP(mod)}} = \alpha E_x^{\mathrm{HF}} + (1-\alpha)E_x^{\mathrm{LSDA}} + 0.9 \times (1-\alpha)\Delta E_X^{\mathrm{B88}} + 0.19 \times E_C^{\mathrm{LSDA}} + 0.81 \times E_c^{\mathrm{LYP}}$$

We benchmarked B3LYP(mod) with α = 0.1, 0.15, and 0.2, ultimately selecting 0.15 for our calculations (Supporting Information Figure S3). Geometry optimizations were carried out using the BFGS[105] algorithm in redundant internal coordinates implemented to the default tolerances of 3×10^{-4} hartree/bohr for the maximum gradient and 5×10^{-6} hartree for the change in energy between steps.

DFT geometry optimizations in which no external force was incorporated were first carried out for Fe^{2+} complexes in singlet, triplet, and quintet states, and Co^{2+} complexes were studied in doublet and quartet states. We eliminated calculations in which the self-consistent field (SCF) failed to converge, and we also considered calculations as having spin-deviation error if the calculated Mulliken spin on the metal deviated from the expected metal spin by more than 1 au. Consequently, we discarded complexes for which geometry optimizations at one or more spin states failed, and we identified the ground spin state of the rest of the complexes (Supporting Information Table S1). For all Fe^{2+} complexes with a low-spin singlet ground state, we found that the high-spin quintet state was lower in energy than the intermediate-spin triplet state. As a result, we calculated the force-free spin-splitting energy as the energy difference between the high-spin and low-spin state for all Fe^{2+} and Co^{2+} complexes with low-spin ground states.

The EFEI method was then used to determine the force-modified ground spin states for low-spin Fe^{2+} and Co^{2+} complexes. We developed a computational workflow that enabled us to quantitatively estimate the critical force for spin-crossover (F_{SCO}), i.e., the threshold force for low-to-high spin transition of the complexes to within a 0.5 nN range (Supporting Information Figure S4). Furthermore, we evaluated the critical force for bond dissociation (F_{De}), i.e., the threshold force under which coordination bonds began to dissociate, for Fe^{2+} and Co^{2+} complexes whose F_{SCO} values were successfully determined. We considered a bond dissociated if the distance between the metal and the coordinating atom exceeded 1.37 times the sum of their covalent radii, and we used the molSimplify[106] package for analysis. We evaluated F_{De} to within a 0.5 nN range with EFEI calculations (Supporting Information Figure S5). During the F_{SCO} evaluation workflow, we found eight complexes that remained LS under X nN, yet in their force-modified ground state under X + 0.5 nN applied force one of more coordination bond has dissociated. We concluded that bond dissociation is likely to occur before the LS-to-HS transition among these complexes and consider them unable to undergo force-activated spin-crossover. Although modeling the dynamic effects of applied forces would potentially lead to increased accuracy, the computational cost of performing dynamical modeling of the large set of complexes becomes prohibitive. Thus, only static DFT and EFEI calculations were conducted.

3. RESULTS AND DISCUSSION

3.1. Selecting Low-Spin Fe^{2+} and Co^{2+} Complexes for EFEI Modeling. We first identified the ground state of the TMCs curated from the CSD to identify structures amenable to force-induced spin crossover (see Sec. 2). From the initial set of 395 TMCs, 201 Fe^{2+} and 100 Co^{2+} complexes with attachment points were successfully optimized in all spin states, allowing for the assignment of their ground states. Although it is possible to envision multiple changes in spin state in response to force, we focused on the most likely spin transitions expected to occur under mechanical force. In previous studies, force has been predominantly leveraged to switch low-spin complexes to high-spin,[43,45,107] and so we discarded complexes that have intermediate-spin or high-spin ground states as indicated by DFT. This led to a final set of 139 Fe^{2+} and 60 Co^{2+} optimized, LS TMCs (Supporting Information Figure S6). In 136 out of 139 Fe^{2+} and 50 out of 60 Co^{2+} TMCs that fit these criteria, all metal-coordinating atoms were nitrogen. As all previously studied (bis)tridentate Fe^{2+} and Co^{2+} complexes exhibiting force-activated spin-crossover have nitrogen as the metal-coordinating atoms,[41−45] we removed the 13 non-nitrogen-coordinated complexes from our set. Nevertheless, these complexes can act as good starting points for expanding the design space of spin-crossover mechanophores in future studies. The remaining 186 complexes were further analyzed by first-principles mechanochemistry calculations. Several Mn^{2+} complexes have also been reported as spin-crossover systems.[108] Utilizing the above workflow, we further examined 31 Mn^{2+} complexes that passed the same filters as and generated a set of 37 uniquely functionalized mechanophore candidates. Of this set of TMCs,

https://doi.org/10.1021/acs.inorgchem.4c04732
Inorg. Chem. 2025, 64, 380−392

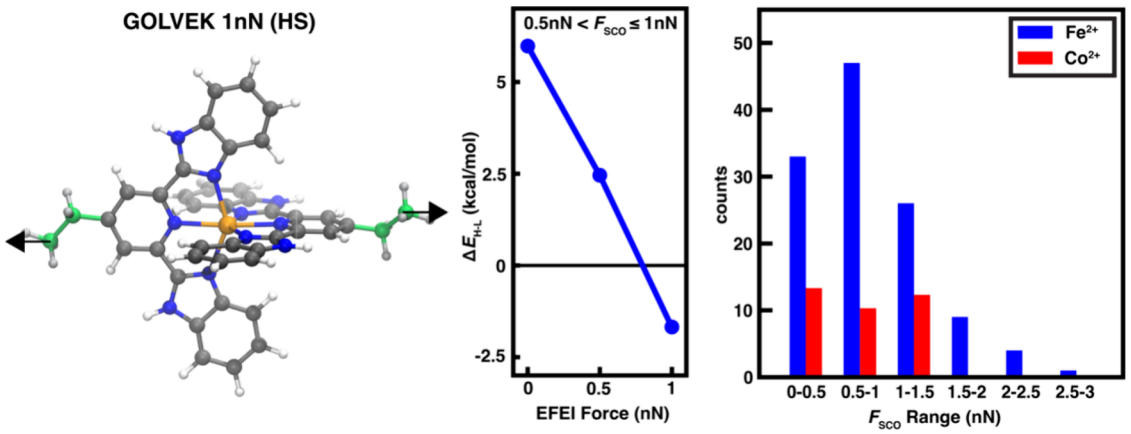

Figure 2. (left) Ground state (HS) structure of an example CSD complex GOLVEK under 1 nN force. (middle) ΔE_{H-L} of GOLVEK under different EFEI forces. (right) Distribution of spin-crossover critical force (F_{SCO}) of Fe^{2+} (blue) and Co^{2+} (red) mechanophores as determined by EFEI. Colors for atoms are as follows: orange for iron, gray for carbon, white for hydrogen, and blue for nitrogen. The carbon and hydrogen atoms in functionalized ethyl groups are colored in light green and light gray for visualization, and the direction of the applied force for each ethyl group is indicated by a black arrow.

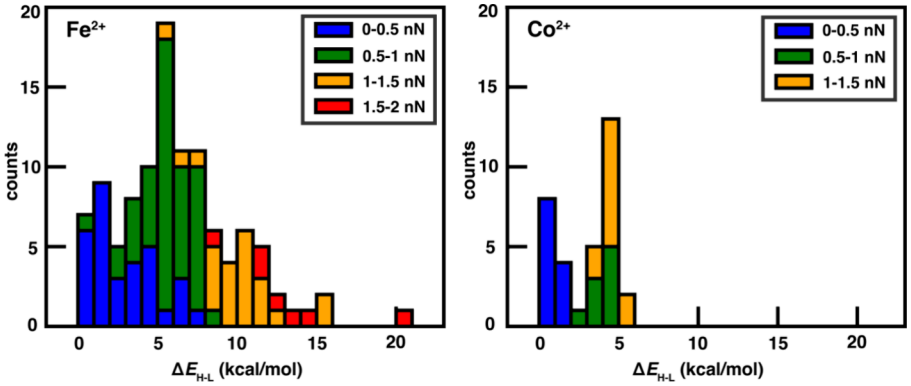

Figure 3. Stacked histograms of spin-splitting energy (ΔE_{H-L}) of *mer*-symmetric (left) Fe^{2+} and (right) Co^{2+} (right) mechanophores, as colored by F_{SCO} (blue for $F_{SCO} \leq 0.5$ nN, green for 0.5 nN < $F_{SCO} \leq 1$ nN, yellow for 1 nN < $F_{SCO} \leq 1.5$ nN, and red for 1.5 nN < $F_{SCO} \leq 2$ nN).

most were successfully calculated in all possible spin states (i.e., 24 of 37), but all of these exhibit an intermediate- or high-spin ground state (Supporting Information Table S1). As a result, Mn^{2+} complexes were not further analyzed in this study.

3.2. Modeling Force-Activated Spin-Crossover in Fe^{2+} and Co^{2+} Mechanophores with First-Principles Calculations. To identify Fe^{2+} and Co^{2+} spin-crossover (SCO) mechanophores that can be activated with a moderate (i.e., ≤ 3.0 nN) force, we developed a computational workflow based on EFEI[67] simulations (Supporting Information Figure S4). Specifically, we computed the force-modified spin-splitting energy of a complex by performing geometry optimizations with EFEI and calculating the adiabatic spin-splitting energy under incrementally increasing values of applied force. We increased the magnitude of applied force to 3 nN if the complex remained low-spin at lower forces in increments of 0.5 nN, and we discarded the complexes in which coordination bond dissociation occurred prior to LS-to-HS transition (see Sec. 2.2). For all complexes in which low-to-high spin transition was promoted by ≤3 nN force, we also determined the critical force for spin-crossover (F_{SCO}), i.e., the threshold force for spin transition of the complexes to within a 0.5 nN range (Figure 2). We successfully computed both properties for 155 out of the 186 Fe^{2+} and Co^{2+} candidates, yielding a set of 120 Fe^{2+} and 35 Co^{2+} mechanophores. On the other hand, we found eight complexes unable to undergo LS-to-HS transition without breaking one or more coordination bonds. The complexes are all *fac*-symmetric, and six exhibit asymmetric-shearing force response which we will further introduce in Sec. 3.2 (Supporting Information Figures S7 and S8). EFEI simulations for the remaining complexes encountered SCF convergence issues (Supporting Information Figure S9). Consistent with the properties of the 199 initial LS complexes that were mostly *mer*-symmetric Fe^{2+}, 141 of the 155 EFEI-characterized complexes are *mer*-symmetric.

The EFEI simulation results revealed that force-activated spin-crossover to high-spin is prevalent (155/163) in low-spin Fe^{2+} and Co^{2+} complexes, and all 155 complexes can act as SCO mechanophores with $F_{SCO} \leq 3$ nN. While most previously-studied complexes exhibiting force-activated spin-crossover have terpyridine ligands, we found that our 155 Fe^{2+} and Co^{2+} mechanophores have significantly increased diversity in ligand chemistry. Many of the mechanophores have the metal center coordinated to other heteroaromatic moieties or even nonheteroaromatic nitrogen (Supporting Information Text S1 and Figures S10−S14). Moreover, 14 of our mechanophores have *fac*-symmetry, a feature not found among known examples (Supporting Information Figures S15 and S16). All Co^{2+} complexes and the majority of Fe^{2+} complexes undergo spin crossover at 1.5 nN or less of applied

https://doi.org/10.1021/acs.inorgchem.4c04732
Inorg. Chem. 2025, 64, 380−392

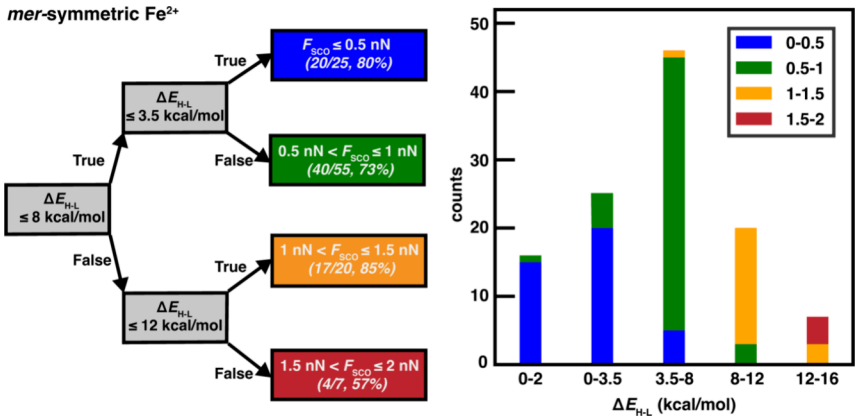

Figure 4. (left) Decision tree classifier diagram of F_{SCO} prediction based on $\Delta E_{H\text{-}L}$ for *mer*-symmetric Fe^{2+} mechanophores. Prediction boundaries are specified, and prediction accuracies are shown. (right) F_{SCO} statistics of *mer*-symmetric Fe^{2+} mechanophores having different $\Delta E_{H\text{-}L}$ values as classified by the decision tree. Statistics of mechanophores with $\Delta E_{H\text{-}L} \leq 2$ kcal/mol that are promising candidates for labile spin-crossover mechanophore are also visualized. The decision tree diagram and the stacked bar plots are colored by F_{SCO} (blue for $F_{SCO} \leq 0.5$ nN, green for 0.5 nN < $F_{SCO} \leq 1$ nN, orange for 1 nN < $F_{SCO} \leq 1.5$ nN, and red for 1.5 nN < $F_{SCO} \leq 2$ nN).

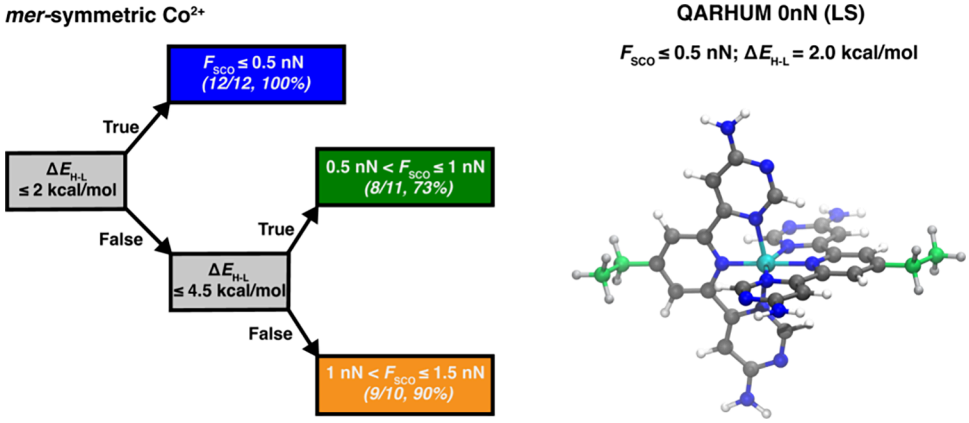

Figure 5. (left) Decision tree classifier diagram of F_{SCO} prediction based on $\Delta E_{H\text{-}L}$ for *mer*-symmetric Co^{2+} mechanophores. Prediction boundaries are specified, and prediction accuracies are shown. The decision tree diagram is colored by F_{SCO} (blue for $F_{SCO} \leq 0.5$ nN, green for 0.5 nN < $F_{SCO} \leq 1$ nN, and orange for 1 nN < $F_{SCO} \leq 1.5$ nN). (right) Force-free ground state (LS) structure of CSD complex QARHUM as an example of a *mer*-symmetric Co^{2+} complex with low $\Delta E_{H\text{-}L}$ thus low F_{SCO}. Colors for atoms are as follows: cyan for cobalt, gray for carbon, white for hydrogen, and blue for nitrogen. The carbon and hydrogen in functionalized ethyl group are colored in light green and light gray for visualization.

mechanical force, and all remaining Fe^{2+} complexes have an $F_{SCO} \leq 3$ nN (Figure 2). Among the Fe^{2+} complexes, 33 require very low force ($F_{SCO} \leq 0.5$ nN) for spin crossover and another 73 require only modest forces (47 0.5 nN < $F_{SCO} \leq 1$ nN and 26 1 nN< $F_{SCO} \leq 1.5$ nN). The F_{SCO} distribution of Co^{2+} complexes is similar to that of Fe^{2+}, with 13 complexes having $F_{SCO} \leq 0.5$ nN, 10 complexes having 0.5 nN < $F_{SCO} \leq 1$ nN, and 12 complexes having 1 nN< $F_{SCO} \leq 1.5$ nN.

The prevalence of spin-crossover induced by low or modest forces among Fe^{2+} and Co^{2+} complexes motivated us to further elucidate the chemical factors distinguishing those that change spin state at very low forces from those that change spin state at higher forces. To begin our analysis of factors influencing force-activated spin-crossover, we first examined the larger *mer*-symmetric grouping, which accounts for more than 90% of the total mechanophores, as response mechanisms can be expected to differ between *mer*-symmetric and *fac*-symmetric mechanophores. We hypothesized that *mer*-symmetric mechanophores with lower spin-splitting energy ($\Delta E_{H\text{-}L}$) would require less force to undergo spin-crossover. If F_{SCO} could be predicted with $\Delta E_{H\text{-}L}$ alone, this would accelerate mechanophore discovery, as the need for extensive EFEI simulations would be eliminated. Our results support this hypothesis for both *mer*-symmetric Fe^{2+} and Co^{2+} mechanophores, as comparison of spin-splitting energies and spin-crossover forces indicates grouping of F_{SCO} for both Fe^{2+} and Co^{2+} complexes according to $\Delta E_{H\text{-}L}$ (Figure 3).

Having identified a clear relationship between F_{SCO} and $\Delta E_{H\text{-}L}$ for *mer*-symmetric Fe^{2+} and Co^{2+} mechanophores, we next aimed to predict the F_{SCO} of these mechanophores based on the force-free $\Delta E_{H\text{-}L}$. We developed decision tree classifiers to quantify such trends using scikit-learn.[109] The two classifiers employ $\Delta E_{H\text{-}L}$ values to estimate the F_{SCO} of *mer*-symmetric Fe^{2+} or Co^{2+} mechanophores, respectively, to the nearest calculated 0.5 nN range (Figures 4 and 5). To avoid overfitting, we rounded the decision boundaries derived by the training algorithm to the nearest 0.5 kcal/mol of $\Delta E_{H\text{-}L}$ and used these rounded values to calculate the prediction accuracies. The classifier for *mer*-symmetric Fe^{2+} mechanophores correctly categorizes F_{SCO} for the majority of complexes with an accuracy of 73% (Figure 4). Furthermore, given our goal of identifying mechanophores with highly labile spin-crossover behavior, we are particularly interested in finding mechanophores with $F_{SCO} \leq 0.5$ nN. We can identify these

https://doi.org/10.1021/acs.inorgchem.4c04732
Inorg. Chem. 2025, 64, 380−392

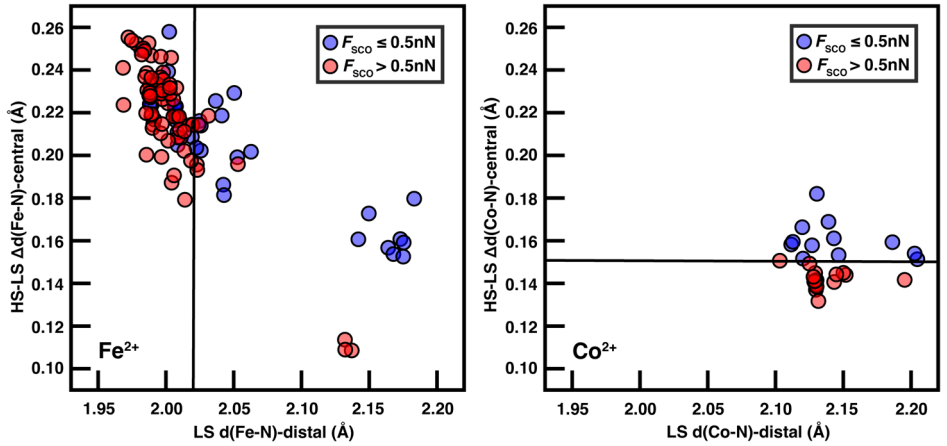

Figure 6. Average distal bond lengths in the force-free LS state (LS d(Fe−N)-distal and LS d(Co−N)-distal) vs differences between average central HS and LS bond lengths (HS-LS Δd(Fe−N)-central and HS-LS Δd(Co−N)-central) for *mer*-symmetric (left) Fe^{2+} mechanophores and (right) Co^{2+} mechanophores that have $F_{SCO} \leq 0.5$ nN or $F_{SCO} > 0.5$ nN. Note that as bond length values are rounded to closest 0.01 Å in decision-tree prediction to maximize generalizability, the categorization visualized here may have subtle differences compared to actual prediction outcomes.

complexes robustly by identifying *mer*-symmetric Fe^{2+} mechanophores with $\Delta E_{H\text{-}L} \leq 2$ kcal/mol, as more than 95% of the complexes with these small $\Delta E_{H\text{-}L}$ values also have F_{SCO} values ≤0.5 nN (Figure 4). The classifier for *mer*-symmetric Co^{2+} mechanophores also correctly categorizes their F_{SCO} values with 73% accuracy (Figure 5 and Supporting Information Figure S17). As with Fe^{2+} complexes, all *mer*-symmetric Co^{2+} mechanophores with $\Delta E_{H\text{-}L} \leq 2$ kcal/mol have F_{SCO} values ≤0.5 nN, facilitating the discovery of highly labile SCO mechanophores. Meanwhile, as *mer*-symmetric Co^{2+} mechanophores have lower $\Delta E_{H\text{-}L}$ than Fe^{2+} ones, we found that the decision boundaries of the Co^{2+} decision tree for less labile mechanophores is lower than those for the Fe^{2+} classifier (Figures 4 and 5). Overall, our analysis reveals an intuitive relationship between critical force for spin-crossover and spin-splitting energy for *mer*-symmetric Fe^{2+} and Co^{2+} complexes, enabling the quantitative predictions of force-activated spin-crossover based on simple force-free DFT calculations alone.

To obtain deeper insights into the behaviors of Fe^{2+} and Co^{2+} mechanophores, we also explored whether the coordination bond lengths in the LS and/or HS states are predictive of F_{SCO}. Predicting spin-crossover behavior with bond length values is desirable, as bond lengths are less sensitive to functional choices compared to $\Delta E_{H\text{-}L}$.[110,111] Analysis of crystal structures in multiple spin states indicates that the LS-to-HS transition typically leads to a bond length increase of 0.2 Å for Fe^{2+} complexes and 0.1 Å for Co^{2+} complexes.[52,91] One might expect that lower than average distortion between the two states, characterized by longer bonds in LS or shorter bonds in HS, could lead to more facile force-induced spin crossover. As elongation of distal and compression of central coordination bonds are generally observed in Fe^{2+} and Co^{2+} complexes due to steric strain and Jahn−Teller distortion,[52,91] we also calculated the averages of two central and four distal bonds in the LS and HS state for each complex. We identified a number of *mer*-symmetric Fe^{2+} mechanophores with LS bond lengths elongated due to steric strain that also exhibit a relatively low F_{SCO} (Supporting Information Figures S18 and S19). Beyond this subset of complexes, it is challenging to distinguish F_{SCO} values of most *mer*-symmetric Fe^{2+} and Co^{2+} complexes using a single bond length factor (Supporting Information Figures S20−S24). Decision tree classifiers built with multiple bond length features are also less predictive than $\Delta E_{H\text{-}L}$-based classifiers (Supporting Information Figures S25 and S26). On the other hand, we find that these decision trees are relatively accurate at categorizing *mer*-symmetric Fe^{2+} and Co^{2+} mechanophores that are the most force responsive (i.e., $F_{SCO} \leq 0.5$ nN). This finding prompted our further analysis on what bond length features are indicative of the most labile SCO mechanophores.

We identified two geometric factors that are predictive of *mer*-symmetric Fe^{2+} and Co^{2+} complexes exhibiting the most reactive mechanochemical responses: the average distal Fe−N coordination bond length in the force-free LS state and the difference in average central Co−N coordination bond length between force-free HS and LS states. Here, central refers to the bond formed between the metal and the middle coordinating atom of the three coordinating atoms on the tridentate ligand, whereas distal can refer to either of the other two coordinating atoms in the tridentate ligand. These two bond length features (i.e., the distal bond average in Fe^{2+} and the central one in Co^{2+}) can be used to accurately categorize Fe^{2+} and Co^{2+} mechanophores with $F_{SCO} \leq 0.5$ nN (Figure 6 and Supporting Information Figures S27 and S28). In fact, all nine *mer*-symmetric Co^{2+} mechanophores with a greater than 0.15 Å difference in central bond length between HS and LS have $F_{SCO} \leq 0.5$ nN, while a large majority (i.e., 77% or 17 out of 22) of *mer*-symmetric Fe^{2+} complexes with larger than 2.02 Å average distal Fe−N bond length in the LS state exhibit $F_{SCO} \leq 0.5$ nN. Additionally, all but three *mer*-symmetric Fe^{2+} complexes have a >0.14 Å HS-LS central bond length difference (Figure 6). The three outliers are all derived from the CSD complex with refcode QERDIB. Discarding these outliers leads to 89% prediction accuracy (17 out of 19) of the most labile *mer*-symmetric Fe^{2+} mechanophores using average LS distal Fe−N bond length alone (Supporting Information Figure S29). The chemical factors leading to central bond compression and distal bond elongation differ between Fe^{2+} and Co^{2+} complexes, and this variation results in differences in geometric factors that are predictive of the most labile Fe^{2+} and Co^{2+} complexes. Because the elongation of distal bonds in Fe^{2+} complexes in the force-free state can be attributed to sterics,[90] longer distal bonds indicate that complexes are likely to favor

https://doi.org/10.1021/acs.inorgchem.4c04732
Inorg. Chem. 2025, 64, 380−392

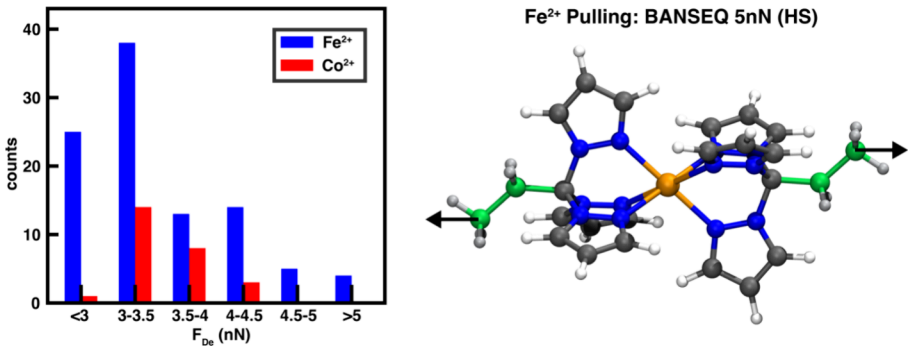

Figure 7. (left) Distribution of bond dissociation critical force (F_{De}) of Fe^{2+} (blue) and Co^{2+} (red) mechanophores as determined by EFEI. (right) Ground state (HS) structure of CSD complex BANSEQ under 5 nN applied force as an example of a pulling-type, *fac*-symmetric Fe^{2+} complex that remained structurally intact under elevated force. Colors for atoms are as follows: orange for iron, gray for carbon, white for hydrogen, blue for nitrogen. The carbon and hydrogen in functionalized ethyl groups are colored in light green and light gray for better visualization.

HS states under force. Although vibrational mode analysis could assess ligand flexibility to complement applied force simulations, the prohibitive computational cost of Hessian calculations on these transition metal complexes of both considerable size and number prohibited our use of this approach. On the other hand, the d^7 Co^{2+} complexes undergo Jahn−Teller compression, leading to shorter central bonds in LS states.[91] A large difference in HS and LS central bond lengths of a complex thus indicates that its LS state is stabilized by a stronger Jahn−Teller effect. If the complex is extended by external force and the Jahn−Teller effect quickly diminishes, then the LS state will become less favorable and LS-to-HS transition will occur. We conclude that, for *mer*-symmetric Fe^{2+} and Co^{2+} mechanophores, force-activated spin-crossover can be quantitatively predicted by spin-splitting energetics, and that complexes with the most labile spin-crossover can be identified by examining distinct bond length factors for Fe^{2+} and Co^{2+} complexes.

While in *mer*-symmetric mechanophores external forces are symmetrically propagated along the entire molecule, force propagation can be expected to be distinct for *fac*-symmetric mechanophores. Here, we observe two different modes through which applied force is propagated based on the position of polymer attachment points: (i) symmetric pulling and (ii) asymmetric shearing (Supporting Information Figures S30 and S31). This distinction arises because, unlike tridentate ligands in *mer*-symmetric mechanophores, tridentate ligands in *fac*-symmetric mechanophores have each coordinating atom located on branches that are bonded to a central atom or group. If the attachment points of a *fac*-symmetric mechanophore are bonded to the central atom or group, then under applied force the mechanophore would be pulled symmetrically. On the other hand, if the attachment points are on the branches, then the mechanophore would undergo asymmetric shearing. Among 12 *fac*-symmetric Fe^{2+} mechanophores, eight are of pulling-type and the remaining four are of shearing-type. For the two *fac*-symmetric Co^{2+} mechanophores, one is of the pulling-type and one is shearing-type.

As symmetric propagation of force along the entire mechanophore leads to less reactive mechanochemical responses, we anticipate that shearing-type *fac*-symmetric mechanophores should exhibit more significant distortion under same magnitude of force. As a result, shearing-type complexes may have lower F_{SCO} than pulling-type ones. By comparing between two *fac*-symmetric Fe^{2+} complexes with similar ligands differing by only one methyl group, we validated that asymmetric shearing leads to more significant elongation of coordination bonds (Supporting Information Figures S30 and S31). We find that all mechanophores in our set that exhibit F_{SCO} > 2 nN are *fac*-symmetric Fe^{2+} mechanophores that exhibit pulling-type force responses, and all shearing-type Fe^{2+} mechanophores exhibit $F_{SCO} \leq 1.5$ nN (Supporting Information Figure S32). Although *fac*-symmetric Fe^{2+} mechanophores tend to exhibit higher ligand field strength and $\Delta E_{H\text{-}L}$, we find the force transduction mechanism (pulling vs shearing) to have a larger influence on F_{SCO}, and comparison between *mer*- and *fac*-symmetric Fe^{2+} complexes based on $\Delta E_{H\text{-}L}$ is thus less applicable (Supporting Information Figures S33 and S34). Also, due to the limited number of complexes, it would be challenging to derive more general conclusions. On the other hand, as we have seen among the *fac*-symmetric complexes that undergo bond dissociation before spin transition, we anticipate that if higher magnitude forces are applied, the two bonds that are most significantly elongated in shearing-type complexes would readily dissociate (Supporting Information Figure S7). Nevertheless, this mechanochemical response can become productive instead of destructive as force can be used to stabilize square-planar coordination, as we will consider further in Sec. 3.3. We anticipate that with further systematic comparison between pulling- and shearing-type *fac*-symmetric mechanophores as well as investigations on *mer*-symmetric mechanophores with non-C_{2v} polymer attachment thus asymmetric force transduction in future studies, further design principles for Fe^{2+} and Co^{2+} mechanophores can be revealed.

3.3. Probing Mechanical Stability of Fe^{2+} and Co^{2+} Spin-Crossover Mechanophores. Dissociation of the ligands in a SCO mechanophore would be problematic for sensing applications because it would not be reversible, so we thus aimed to identify Fe^{2+} and Co^{2+} complexes with labile spin-crossover that also had good mechanical robustness for reversible coordination bond extension without subsequent dissociation. Consequently, we evaluated the critical force for bond dissociation (F_{De}), i.e., the threshold force under which coordination bonds began to dissociate (see Sec. 2.2), for all 120 Fe^{2+} and 35 Co^{2+} mechanophores. We evaluated this force to within a 0.5 nN interval successfully for 125 of 155 complexes, while EFEI simulation for the remaining complexes encountered SCF convergence issues (Supporting Information Figures S5 and S35). For this set, we found that 27 complexes remain structurally intact without bond dissociation under applied force of 4 nN or higher, and the remaining >70% of

https://doi.org/10.1021/acs.inorgchem.4c04732
Inorg. Chem. 2025, 64, 380−392

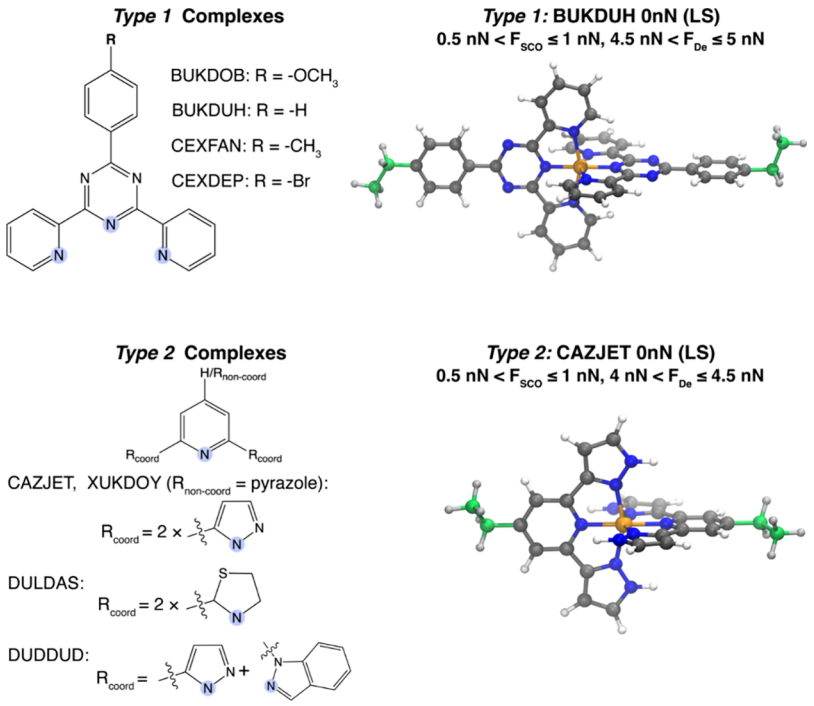

Figure 8. (left, top) Chemical structures of ligands in *Type 1* Fe^{2+} complexes that contain conjugated triazine, pyridine, and benzene rings. (right, top) Ground state (LS), force-free structure of one complex (CSD refcode: BUKDUH) as an example of a *Type 1* complex. (left, bottom) Chemical structures of ligands in *Type 2* Fe^{2+} complexes that contain one pyridine conjugated to heteroaromatic rings. (right, bottom) Ground state (LS) structure of one complex (CSD refcode: CAZJET) as an example of a *Type 2* Fe^{2+} complex that exhibits low F_{SCO} and high F_{De}. Colors for atoms are as follows: orange for iron, gray for carbon, white for hydrogen, and blue for nitrogen. The carbon and hydrogen in functionalized ethyl groups are colored in light green and light gray for better visualization.

mechanophores have $F_{De} \leq 4$ nN (Figure 7). Moreover, all four complexes that exhibit $F_{De} > 5$ nN are all pulling-type, *fac*-symmetric Fe^{2+} species (Figure 7 and Supporting Information Figure S36). Although symmetric force propagation along the entire complex causes pulling-type, *fac*-symmetric complexes to be less force-responsive in their spin-crossover behavior, it also makes these complexes particularly robust under mechanical loading. We expect these pulling-type complexes to be building blocks of polymer networks with high tearing energy and outstanding mechanical strength.[112]

While terpyridine ligands have been studied previously in complexes exhibiting force-activated spin-crossover,[41−43,45] replacing the central or both distal pyridine groups results in ligands and mechanophores simultaneously exhibiting labile spin-crossover and good mechanical robustness. Among all mechanically robust mechanophores with $F_{De} > 4$ nN, we identified nine *mer*-symmetric Fe^{2+} and two *mer*-symmetric Co^{2+} mechanophores that exhibit $F_{SCO} \leq 1$ nN. Based on ligand structures, the Fe^{2+} mechanophores can predominantly be categorized into two types. In the four *Type 1* complexes, the ligands are derivatives of 2,6-bis(pyridine)-1-phenyltriazine (Figure 8 and Supporting Information Figures S37 and S38). The *Type 1* CSD complex with refcode BUKDOB has the lowest F_{SCO} ($F_{SCO} \leq 0.5$ nN) and highest F_{De} (4.5 nN < $F_{De} \leq$ 5 nN) (Figure 8). One Co^{2+} mechanophore, CSD complex TABDOP, also has a ligand with the bis(pyridine)-triazine motif (Supporting Information Figure S39). In the four *Type 2* complexes, the central and distal Fe−N bonds are formed with nitrogen in conjugated pyridine and five-membered rings with two heteroatoms (Figure 8 and Supporting Information Figure S40). Additionally, in the last Fe^{2+} mechanophore, the central and one distal Fe−N bonds are formed with pyridine rings fused in a phenanthroline group, and the other distal Fe−N bond is formed with a tetrazole bonded to the phenanthroline (Supporting Information Figure S41). Finally, in the other Co^{2+} mechanophore, all Co−N coordination bonds are formed with pyridine groups, yet the pyridine rings are bonded not by C−C single bonds but through NH bridges (Supporting Information Figure S42). These ligands can act as starting points for further systematic discovery of spin-crossover Fe^{2+} mechanophores and especially Co^{2+} mechanophores.

Due to asymmetric propagation of applied force on two coordination bonds, shearing-type *fac*-symmetric mechanophores are less mechanically robust compared to pulling-type complexes, leading to bond breaking in three Fe^{2+} and four Co^{2+} complexes at moderate forces. Nevertheless, this bond rupture could enable the design of functional materials, as mechanical loading would promote octahedral-to-square-planar conformation switching in shearing-type mechanophores and stabilize the resulting square planar complex. We found that with 3 nN applied force, all three Fe^{2+} and three out of four Co^{2+} shearing-type complexes evolve into a distorted square-planar geometry (Figure 9 and Supporting Information Text S2). For one complex, an applied force of 5 nN is needed to promote such structural evolution (Supporting Information Figure S43). In all seven complexes, this transition is characterized by a coplanar arrangement of the metal atom and the four remaining coordinating nitrogen atoms. Although the average angle between two adjacent coordination bonds is 90°, the angles between two adjacent bonds in the same ligand are compressed. This means that angles between the adjacent bonds in different ligands are then increased in a compensatory fashion (Figure 9).

https://doi.org/10.1021/acs.inorgchem.4c04732
Inorg. Chem. 2025, 64, 380−392

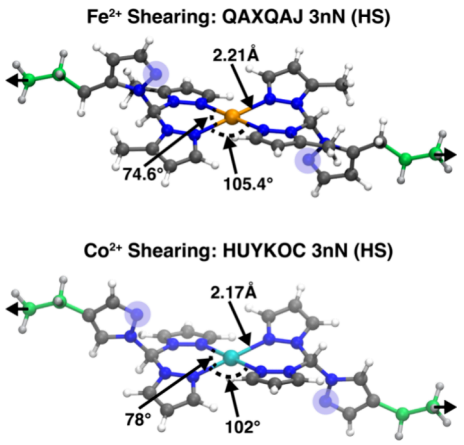

Figure 9. Ground state (HS, square planar) structure of one Fe^{2+} complex (CSD refcode: QAXQAJ) (top) and a Co^{2+} complex (CSD refcode: HUYKOC) (bottom) under 3 nN applied force as examples of shearing-type, *fac*-symmetric Fe^{2+} and Co^{2+} complexes. Relevant bond lengths and bond angles in each complex are labeled. Nitrogen atoms forming coordination bonds in force-free structures that are dissociated upon applied force are highlighted. Colors for atoms are as follows: orange for iron, cyan for cobalt, gray for carbon, white for hydrogen, and blue for nitrogen. The carbon and hydrogen in functionalized ethyl groups are colored in light green and light gray for better visualization.

We observe that all seven conformation-switching complexes have similar ligands. The ligands are all comprised of three pyrazole, imidazole, or pyridine rings bonded to a linking atom, and coordination bonds are formed between the metal center and a nitrogen in each of the three heteroaromatic rings. In all but one complex, four pyrazole or four imidazole rings remain coordinated to the Fe^{2+} or Co^{2+} center in the distorted square-planar complexes, and the four coordination bonds in each complex have similar lengths (Figure 9 and Supporting Information Figures S44−S47). In one complex (CSD refcode: DIFBAX), two pyrazole and two pyridine rings remained coordinated to the metal center, and the bonds formed with nitrogen in pyridine are 0.12 Å longer than bonds formed with nitrogen in pyrazole (Supporting Information Figure S44). Moreover, in six out of the seven complexes, the pulling points are attached to pyrazole or imidazole rings coordinated to the metal center in the force-free structures. In one complex (CSD refcode: QIZJIU) mentioned earlier for its high 5 nN force required for structural evolution, this can be attributed to the fact that the pulling points are attached to pyridine rings instead. Here, the higher force could arise from the steric hindrance of ligand rotation experienced when displacing a six-membered ring from the metal center (Supporting Information Figures S43). In their force-free HS states, the seven complexes have average bond lengths between 2.13 and 2.20 Å, which are similar to their bond lengths in the distorted square planar geometry (2.10 to 2.26 Å). In fact, in five out of seven complexes, the force-free and force-modified bonds differ by less than 0.03 Å (Supporting Information Table S2). In two complexes, the square-planar structure has even shorter bond lengths, suggesting favorability of forming the square-planar conformation. Based on our findings, we envision a broad design space of shearing-type ligands for conformation switching complexes, and we consider these complexes as promising candidates for mechanically activated catalysts that have broad applications in polymer science.[15,16,113] On the other hand, possible coordination of the activated square-planar site with solvent molecules should be further examined, and these complexes are thus potentially more compatible with dry polymer networks.

4. CONCLUSIONS

We developed a strategy for computational discovery of synthetically accessible transition metal complexes with the potential to change spin in response to mechanical force. From a set of complexes mined from the CSD, we identified 199 synthetically accessible LS homoleptic (bis)tridentate Fe^{2+} and Co^{2+} complexes that are feasible candidates for spin-crossover mechanophores. By simulating the application of mechanical force with EFEI, we found that force-activated spin-crossover from LS to HS is prevalent among the complexes. We revealed that among the majority of *mer*-symmetric complexes, labile force-activated spin-crossover is associated with low values of force-free spin-splitting energy. From this insight, we trained decision tree classifiers that enable quantitative prediction of the critical force for spin-crossover based on spin-splitting energy and, thus, simple force-free DFT. Furthermore, we found that the most reactive *mer*-symmetric Fe^{2+} and Co^{2+} spin-crossover mechanophores can be predicted using the LS distal bond lengths and the HS central bond length, which are easy to compute and less sensitive to DFT functional choice than the spin-splitting energy. Although interactions with the polymer network environment could further influence their mechanochemical response, identification of these labile spin-crossover mechanophores is expected to guide pathways in further synthetic studies and experimental examination.

To understand the factors leading to facile spin crossover but high mechanical stability, we focused on the 11 Fe^{2+} and Co^{2+} complexes that can be activated for spin-crossover at 0.5 nN force while remaining structurally intact under higher mechanical loadings. We found that ligands in these complexes are made by substituting the central or both distal groups in the previously studied terpyridine ligands or by inserting NH bridges between the pyridines. This class of spin-crossover transition metal mechanophores broadens the range of mechanical responses beyond what is possible with current organic mechanophores, and the above-mentioned 11 complexes are promising candidates for follow-up synthesis and characterization. In addition, we discovered a second class of promising complexes comprising certain *fac*-symmetric ligands, wherein applied force led to not only spin-crossover but also a transition to square-planar geometries upon rupture of two coordination bonds. This makes these latter complexes promising candidates for future study to identify complexes with catalytic centers that can be mechanically activated.

We envision future studies that expand upon the present study by enlarging the chemical space surveyed. In exploring an even greater number of compounds, we anticipate further refinement of design principles for transition metal mechanophores exhibiting labile spin-crossover or identifying reactions that can benefit from complexes that are "unmasked" by mechanical force, paving the way for their development as versatile building blocks for smart polymer materials and molecular devices.

■ ASSOCIATED CONTENT

Data Availability Statement

All data is available in the main text, Supporting Information, and Zenodo repository.[114]

https://doi.org/10.1021/acs.inorgchem.4c04732
Inorg. Chem. 2025, 64, 380−392

Supporting Information

The Supporting Information is available free of charge at https://pubs.acs.org/doi/10.1021/acs.inorgchem.4c04732.

Metal identity statistics of all homoleptic, tridentate complexes in CSD; example of multiple mechanophores generated from one complex; benchmarking of HF exchange percentage in the B3LYP(mod)-D3BJ functional; EFEI calculation workflow for F_{SCO} evaluation; EFEI calculation workflow for F_{De} evaluation; statistics of DFT optimization results of Fe^{2+} and Co^{2+} complexes; statistics of DFT optimization results of Fe^{2+}, Co^{2+}, and Mn^{2+} complexes; examples of shearing-type complexes that undergo bond dissociation; structures of other fac-symmetric complexes that undergo bond dissociation; statistics of successful EFEI simulation results of Fe^{2+} and Co^{2+} complexes; ligand structure comparison with previous reported SCO systems; example of complexes with metal-pyridine coordination; example of complexes with other metal-heteroaromatic ring coordination; example of complexes with Schiff base ligands; example of complexes with DAPH ligands; example of complexes with 2,6-(bis)-oxazoline/thiazoline ligands; example of fac-symmetric complexes with full metal-heteroaromatic bonds; structures of fac-symmetric complexes with other ligands; F_{SCO} statistics of *mer*-symmetric Co^{2+} complexes in $\Delta E_{H\text{-}L}$ intervals; LS bond length statistics of *mer*-symmetric complexes; example of *mer*-symmetric Fe^{2+} complexes with long-arm ligands; HS bond length statistics of *mer*-symmetric complexes; LS central bond length statistics of *mer*-symmetric complexes; HS central bond length statistics of *mer*-symmetric complexes; LS distal bond length statistics of *mer*-symmetric complexes; HS distal bond length statistics of *mer*-symmetric complexes; bond length features decision tree for *mer*-symmetric Fe^{2+} complexes; bond length features decision tree for *mer*-symmetric Co^{2+} complexes; bond length decision tree for labile *mer*-symmetric Fe^{2+} complexes; bond length decision tree for labile mer-symmetric Co^{2+} complexes; structures of three QER-DIB-derived Fe^{2+} mechanophores; example of shearing-type fac-symmetric Fe^{2+} complexes; example of pulling-type fac-symmetric Fe^{2+} complexes; F_{SCO} of shearing- and pulling-type fac-symmetric Fe^{2+} complexes; statistics of successful EFEI simulations under elevated forces; structures of three shearing-type, fac-symmetric Fe^{2+} complexes; structures of two type 1 Fe^{2+} complexes with similar structures; structures of two type 1 Fe^{2+} complexes; structure of Co^{2+} complex TABDOP analogous to type 1 complexes; structures of three type 2 Fe^{2+} complexes; structure of Fe^{2+} complex QIDJOD that exhibit low F_{SCO} and high F_{De}; structures of Co^{2+} complex GEYCAQ that exhibit low F_{SCO} and high F_{De}; Procedures for modeling shearing-type Co^{2+} complexes upon 3 nN force; structures of Co^{2+} complex QIZJIU upon 3 nN and 5 nN force; square-planar structure of Fe^{2+} complex DIFBAX upon 3 nN force; square-planar geometry of Fe^{2+} complex YUJBUB upon 3 nN force; square-planar geometry of Co^{2+} complex KIGDIO upon 3 nN force; square-planar geometry of Co^{2+} complex AJUMEY upon 3 nN force; average HS bond lengths of shearing-type complexes upon 0/3/5 nN force (PDF)

AUTHOR INFORMATION

Corresponding Author

Heather J. Kulik − *Department of Chemistry and Department of Chemical Engineering, Massachusetts Institute of Technology, Cambridge, Massachusetts 02139, United States; NSF Center for the Chemistry of Molecularly Optimized Networks, Duke University, Durham, North Carolina 27708, United States;* orcid.org/0000-0001-9342-0191; Email: hjkulik@mit.edu

Authors

Xiao Huang − *Department of Chemistry and Department of Chemical Engineering, Massachusetts Institute of Technology, Cambridge, Massachusetts 02139, United States; NSF Center for the Chemistry of Molecularly Optimized Networks, Duke University, Durham, North Carolina 27708, United States*

Ilia Kevlishvili − *Department of Chemical Engineering, Massachusetts Institute of Technology, Cambridge, Massachusetts 02139, United States; NSF Center for the Chemistry of Molecularly Optimized Networks, Duke University, Durham, North Carolina 27708, United States;* orcid.org/0000-0001-8133-4165

Stephen L. Craig − *NSF Center for the Chemistry of Molecularly Optimized Networks and Department of Chemistry, Duke University, Durham, North Carolina 27708, United States;* orcid.org/0000-0002-8810-0369

Complete contact information is available at: https://pubs.acs.org/10.1021/acs.inorgchem.4c04732

Author Contributions

Xiao Huang: data curation, investigation, conceptualization, writing (original draft preparation), and visualization; Ilia Kevlishvili: data curation, conceptualization, and writing (reviewing and editing); Stephen L. Craig: supervision and writing (reviewing and editing). Heather J. Kulik: writing (reviewing and editing), supervision, and conceptualization.

Notes

The authors declare no competing financial interest.

ACKNOWLEDGMENTS

This work was supported by the NSF Center for the Chemistry of Molecularly Optimized Networks (MONET), CHE-2116298. This work used Expanse at the San Diego Supercomputing Center through allocation CHE140073 from the Advanced Cyberinfrastructure Coordination Ecosystem: Services and Support (ACCESS) program, which is supported by National Science Foundation Grants nos. 2138259, 2138286, 2138307, 2137603, and 2138296. The authors acknowledge David Kastner, Gianmarco Terrones, and Adam H. Steeves for providing critical reading of the manuscript and suggestions on figure preparation.

REFERENCES

(1) Li, J.; Nagamani, C.; Moore, J. S. Polymer Mechanochemistry: From Destructive to Productive. *Acc. Chem. Res.* **2015**, *48*, 2181−2190.

(2) Caruso, M. M.; Davis, D. A.; Shen, Q.; Odom, S. A.; Sottos, N. R.; White, S. R.; Moore, J. S. Mechanically-Induced Chemical Changes in Polymeric Materials. *Chem. Rev.* **2009**, *109*, 5755−5798.

(3) Black, A. L.; Lenhardt, J. M.; Craig, S. L. From Molecular Mechanochemistry to Stress-Responsive Materials. *J. Mater. Chem.* **2011**, *21*, 1655−1663.

(4) Lloyd, E. M.; Vakil, J. R.; Yao, Y. X.; Sottos, N. R.; Craig, S. L. Covalent Mechanochemistry and Contemporary Polymer Network Chemistry: A Marriage in the Making. *J. Am. Chem. Soc.* **2023**, *145*, 751−768.
(5) Davis, D. A.; Hamilton, A.; Yang, J. L.; Cremar, L. D.; Van Gough, D.; Potisek, S. L.; Ong, M. T.; Braun, P. V.; Martinez, T. J.; White, S. R.; et al. Force-Induced Activation of Covalent Bonds in Mechanoresponsive Polymeric Materials. *Nature* **2009**, *459*, 68−72.
(6) Gossweiler, G. R.; Hewage, G. B.; Soriano, G.; Wang, Q. M.; Welshofer, G. W.; Zhao, X. H.; Craig, S. L. Mechanochemical Activation of Covalent Bonds in Polymers with Full and Repeatable Macroscopic Shape Recovery. *ACS Macro Lett.* **2014**, *3*, 216−219.
(7) Robb, M. J.; Kim, T. A.; Halmes, A. J.; White, S. R.; Sottos, N. R.; Moore, J. S. Regioisomer-Specific Mechanochromism of Naphthopyran in Polymeric Materials. *J. Am. Chem. Soc.* **2016**, *138*, 12328−12331.
(8) Sagara, Y.; Yamane, S.; Mitani, M.; Weder, C.; Kato, T. Mechanoresponsive Luminescent Molecular Assemblies: An Emerging Class of Materials. *Adv. Mater.* **2016**, *28*, 1073−1095.
(9) Sun, Y.; Wang, K.; Huang, X.; Wei, S.; Contreras, E.; Jain, P. K.; Campos, L. M.; Kulik, H. J.; Moore, J. S. Caged AIEgens: Multicolor and White Emission Triggered by Mechanical Activation. *J. Am. Chem. Soc.* **2024**, *146*, 27117−27126.
(10) Sun, Y. Y.; Neary, W. J.; Burke, Z. P.; Qian, H.; Zhu, L. Y.; Moore, J. S. Mechanically Triggered Carbon Monoxide Release with Turn-on Aggregation-Induced Emission. *J. Am. Chem. Soc.* **2022**, *144*, 1125−1129.
(11) Sun, Y.; Neary, W. J.; Huang, X.; Kouznetsova, T. B.; Ouchi, T.; Kevlishvili, I.; Wang, K.; Chen, Y.; Kulik, H. J.; Craig, S. L.; et al. A Thermally Stable SO2-Releasing Mechanophore: Facile Activation, Single-Event Spectroscopy, and Molecular Dynamic Simulations. *J. Am. Chem. Soc.* **2024**, *146*, 10943−10952.
(12) Versaw, B. A.; Zeng, T.; Hu, X. R.; Robb, M. J. Harnessing the Power of Force: Development of Mechanophores for Molecular Release. *J. Am. Chem. Soc.* **2021**, *143*, 21461−21473.
(13) Hu, Y. X.; Lin, Y. J.; Craig, S. L. Mechanically Triggered Polymer Deconstruction through Mechanoacid Generation and Catalytic Enol Ether Hydrolysis. *J. Am. Chem. Soc.* **2024**, *146*, 2876−2881.
(14) Hu, Y. X.; Wang, L. Q.; Kevlishvili, I.; Wang, S.; Chiou, C. Y.; Shieh, P.; Lin, Y. J.; Kulik, H. J.; Johnson, J. A.; Craig, S. L. Self-Amplified HF Release and Polymer Deconstruction Cascades Triggered by Mechanical Force. *J. Am. Chem. Soc.* **2024**, *146*, 10115−10123.
(15) Piermattei, A.; Karthikeyan, S.; Sijbesma, R. P. Activating Catalysts with Mechanical Force. *Nat. Chem.* **2009**, *1*, 133−137.
(16) Michael, P.; Binder, W. H. A Mechanochemically Triggered "Click" Catalyst. *Angew. Chem. Int. Edit* **2015**, *54*, 13918−13922.
(17) Hickenboth, C. R.; Moore, J. S.; White, S. R.; Sottos, N. R.; Baudry, J.; Wilson, S. R. Biasing Reaction Pathways with Mechanical Force. *Nature* **2007**, *446*, 423−427.
(18) Lenhardt, J. M.; Ong, M. T.; Choe, R.; Evenhuis, C. R.; Martinez, T. J.; Craig, S. L. Trapping a Diradical Transition State by Mechanochemical Polymer Extension. *Science* **2010**, *329*, 1057−1060.
(19) Liu, Y.; Holm, S.; Meisner, J.; Jia, Y.; Wu, Q.; Woods, T. J.; Martinez, T. J.; Moore, J. S. Flyby Reaction Trajectories: Chemical Dynamics under Extrinsic Force. *Science* **2021**, *373*, 208.
(20) Ramirez, A. L. B.; Kean, Z. S.; Orlicki, J. A.; Champhekar, M.; Elsakr, S. M.; Krause, W. E.; Craig, S. L. Mechanochemical Strengthening of a Synthetic Polymer in Response to Typically Destructive Shear Forces. *Nat. Chem.* **2013**, *5*, 757−761.
(21) Wang, S.; Hu, Y. X.; Kouznetsova, T. B.; Sapir, L.; Chen, D.; Herzog-Arbeitman, A.; Johnson, J. A.; Rubinstein, M.; Craig, S. L. Facile Mechanochemical Cycloreversion of Polymer Cross-Linkers Enhances Tear Resistance. *Science* **2023**, *380*, 1248−1252.
(22) Kean, Z. S.; Niu, Z. B.; Hewage, G. B.; Rheingold, A. L.; Craig, S. L. Stress-Responsive Polymers Containing Cyclobutane Core Mechanophores: Reactivity and Mechanistic Insights. *J. Am. Chem. Soc.* **2013**, *135*, 13598−13604.
(23) Wang, Z.; Zheng, X.; Ouchi, T.; Kouznetsova, T. B.; Beech, H. K.; Av-Ron, S.; Matsuda, T.; Bowser, B. H.; Wang, S.; Johnson, J. A.; Kalow, J. A.; Olsen, B. D.; Gong, J. P.; Rubinstein, M.; Craig, S. L.; et al. Toughening Hydrogels through Force-Triggered Chemical Reactions That Lengthen Polymer Strands. *Science* **2021**, *374*, 193.
(24) Yao, Y.; McFadden, M. E.; Luo, S. M.; Barber, R. W.; Kang, E.; Bar-Zion, A.; Smith, C. A. B.; Jin, Z.; Legendre, M.; Ling, B.; Malounda, D.; Torres, A.; Hamza, T.; Edwards, C. E. R.; Shapiro, M. G.; Robb, M. J.; et al. Remote Control of Mechanochemical Reactions under Physiological Conditions Using Biocompatible Focused Ultrasound. *Proc. Natl. Acad. Sci. U. S. A.* **2023**, *120*, No. e2309822120.
(25) Chen, L.; Nixon, R.; De Bo, G. Force-Controlled Release of Small Molecules with a Rotaxane Actuator. *Nature* **2024**, *628*, 320.
(26) Diesendruck, C. E.; Peterson, G. I.; Kulik, H. J.; Kaitz, J. A.; Mar, B. D.; May, P. A.; White, S. R.; Martínez, T. J.; Boydston, A. J.; Moore, J. S. Mechanically Triggered Heterolytic Unzipping of a Low-Ceiling-Temperature Polymer. *Nat. Chem.* **2014**, *6*, 623−629.
(27) Lin, Y. J.; Kouznetsova, T. B.; Craig, S. L. Mechanically Gated Degradable Polymers. *J. Am. Chem. Soc.* **2020**, *142*, 2105−2109.
(28) Wang, Z. J.; Wang, S.; Jiang, J. L.; Hu, Y. X.; Nakajima, T.; Maeda, S.; Craig, S. L.; Gong, J. P. Effect of the Activation Force of Mechanophore on Its Activation Selectivity and Efficiency in Polymer Networks. *J. Am. Chem. Soc.* **2024**, *146*, 13336−13346.
(29) Chen, Y. J.; Mellot, G.; van Luijk, D.; Creton, C.; Sijbesma, R. P. Mechanochemical Tools for Polymer Materials (Vol 50, Pg 4100, 2021). *Chem. Soc. Rev.* **2021**, *50*, 6659−6660.
(30) Ghanem, M. A.; Basu, A.; Behrou, R.; Boechler, N.; Boydston, A. J.; Craig, S. L.; Lin, Y. J.; Lynde, B. E.; Nelson, A.; Shen, H.; et al. The Role of Polymer Mechanochemistry in Responsive Materials and Additive Manufacturing. *Nat. Rev. Mater.* **2021**, *6*, 84−98.
(31) Qi, Q. K.; Sekhon, G.; Chandradat, R.; Ofodum, N. M.; Shen, T. R.; Scrimgeour, J.; Joy, M.; Wriedt, M.; Jayathirtha, M.; Darie, C. C.; et al. Force-Induced near-Infrared Chromism of Mechanophore-Linked Polymers. *J. Am. Chem. Soc.* **2021**, *143*, 17337−17343.
(32) Yang, F.; Li, X.; Chen, Y. A Chromic and near-Infrared Emissive Mechanophore Serving as a Versatile Force Meter in Micelle-Hydrogel Composites. *Adv. Opt Mater.* **2022**, *10*, No. 2102552.
(33) Balkenende, D. W. R.; Coulibaly, S.; Balog, S.; Simon, Y. C.; Fiore, G. L.; Weder, C. Mechanochemistry with Metallosupramolecular Polymers. *J. Am. Chem. Soc.* **2014**, *136*, 10493−10498.
(34) Johnson, P. N.; Yao, Y. X.; Huang, X.; Kevlishvili, I.; Schrettl, S.; Weder, C.; Kulik, H. J.; Craig, S. L. Metal Identity Effects in the Fracture Behavior of Coordinatively Crosslinked Elastomers. *Polymer* **2023**, *285*, No. 126337.
(35) Kean, Z. S.; Hawk, J. L.; Lin, S.; Zhao, X.; Sijbesma, R. P.; Craig, S. L. Increasing the Maximum Achievable Strain of a Covalent Polymer Gel through the Addition of Mechanically Invisible Cross-Links. *Adv. Mater.* **2014**, *26*, 6013.
(36) Cha, Y. J.; Zhu, T. Y.; Sha, Y.; Lin, H. N.; Hwang, J.; Seraydarian, M.; Craig, S. L.; Tang, C. B. Mechanochemistry of Cationic Cobaltocenium Mechanophore. *J. Am. Chem. Soc.* **2021**, *143*, 11871−11878.
(37) Zhang, Y.; Wang, Z.; Kouznetsova, T. B.; Sha, Y.; Xu, E.; Shannahan, L.; Fermen-Coker, M.; Lin, Y.; Tang, C.; Craig, S. L. Distal Conformational Locks on Ferrocene Mechanophores Guide Reaction Pathways for Increased Mechanochemical Reactivity. *Nat. Chem.* **2021**, *13*, 56.
(38) Filonenko, G. A.; Sun, D. P.; Weber, M.; Müller, C.; Pidko, E. A. Multicolor Organometallic Mechanophores for Polymer Imaging Driven by Exciplex Level Interactions. *J. Am. Chem. Soc.* **2019**, *141*, 9687−9692.
(39) Di Giannantonio, M.; Ayer, M. A.; Verde-Sesto, E.; Lattuada, M.; Weder, C.; Fromm, K. M. Triggered Metal Ion Release and Oxidation: Ferrocene as a Mechanophore in Polymers. *Angew. Chem. Int. Edit* **2018**, *57*, 11445−11450.

https://doi.org/10.1021/acs.inorgchem.4c04732
Inorg. Chem. 2025, 64, 380−392

(40) Mareliati, M.; Tadiello, L.; Guerra, S.; Giannini, L.; Schrettl, S.; Weder, C. Metal-Ligand Complexes as Dynamic Sacrificial Bonds in Elastic Polymers. *Macromolecules* **2022**, *55*, 5164−5175.
(41) Baadji, N.; Sanvito, S. Giant Resistance Change across the Phase Transition in Spin-Crossover Molecules. *Phys. Rev. Lett.* **2012**, *108*, No. 217201.
(42) Harzmann, G. D.; Frisenda, R.; van der Zant, H. S. J.; Mayor, M. Single-Molecule Spin Switch Based on Voltage-Triggered Distortion of the Coordination Sphere. *Angew. Chem. Int. Edit* **2015**, *54*, 13425−13430.
(43) Frisenda, R.; Harzmann, G. D.; Celis Gil, J. A.; Thijssen, J. M.; Mayor, M.; van der Zant, H. S. J. Stretching-Induced Conductance Increase in a Spin-Crossover Molecule. *Nano Lett.* **2016**, *16*, 4733−4737.
(44) Kuang, G. W.; Zhang, Q. S.; Lin, T.; Pang, R.; Shi, X. Q.; Xu, H.; Lin, N. Mechanically-Controlled Reversible Spin Crossover of Single Fe-Porphyrin Molecules. *ACS Nano* **2017**, *11*, 6295−6300.
(45) Parks, J. J.; Champagne, A. R.; Costi, T. A.; Shum, W. W.; Pasupathy, A. N.; Neuscamman, E.; Flores-Torres, S.; Cornaglia, P. S.; Aligia, A. A.; Balseiro, C. A.; et al. Mechanical Control of Spin States in Spin-1 Molecules and the Underscreened Kondo Effect. *Science* **2010**, *328*, 1370−1373.
(46) Venkataramani, S.; Jana, U.; Dommaschk, M.; Sönnichsen, F. D.; Tuczek, F.; Herges, R. Magnetic Bistability of Molecules in Homogeneous Solution at Room Temperature. *Science* **2011**, *331*, 445−448.
(47) Jeon, I. R.; Park, J. G.; Haney, C. R.; Harris, T. D. Spin Crossover Iron(II) Complexes as Paracest MRI Thermometers. *Chem. Sci.* **2014**, *5*, 2461−2465.
(48) Enriquez-Cabrera, A.; Rapakousiou, A.; Piedrahita Bello, M.; Molnár, G.; Salmon, L.; Bousseksou, A. Spin Crossover Polymer Composites, Polymers and Related Soft Materials. *Coordin. Chem. Rev.* **2020**, *419*, No. 213396.
(49) Rat, S.; Piedrahita-Bello, M.; Salmon, L.; Molnár, G.; Demont, P.; Bousseksou, A. Coupling Mechanical and Electrical Properties in Spin Crossover Polymer Composites. *Adv. Mater.* **2018**, *30*, No. 1705275.
(50) Piedrahita-Bello, M.; Martin, B.; Salmon, L.; Molnár, G.; Demont, P.; Bousseksou, A. Mechano-Electric Coupling in P(VDF-TrFE)/Spin Crossover Composites. *J. Mater. Chem. C* **2020**, *8*, 6042−6051.
(51) Janet, J. P.; Chan, L.; Kulik, H. J. Accelerating Chemical Discovery with Machine Learning: Simulated Evolution of Spin Crossover Complexes with an Artificial Neural Network. *J. Phys. Chem. Lett.* **2018**, *9*, 1064−1071.
(52) Taylor, M. G.; Yang, T.; Lin, S.; Nandy, A.; Janet, J. P.; Duan, C. R.; Kulik, H. J. Seeing Is Believing: Experimental Spin States from Machine Learning Model Structure Predictions. *J. Phys. Chem. A* **2020**, *124*, 3286−3299.
(53) Vennelakanti, V.; Kilic, I. B.; Terrones, G. G.; Duan, C. R.; Kulik, H. J. Machine Learning Prediction of the Experimental Transition Temperature of Fe(II) Spin-Crossover Complexes. *J. Phys. Chem. A* **2024**, *128*, 204−216.
(54) Nandy, A.; Zhu, J. Z.; Janet, J. P.; Duan, C. R.; Getman, R. B.; Kulik, H. J. Machine Learning Accelerates the Discovery of Design Rules and Exceptions in Stable Metal-Oxo Intermediate Formation. *ACS Catal.* **2019**, *9*, 8243−8255.
(55) Nandy, A.; Kulik, H. J. Why Conventional Design Rules for C-H Activation Fail for Open-Shell Transition-Metal Catalysts. *ACS Catal.* **2020**, *10*, 15033−15047.
(56) Nandy, A.; Duan, C.; Goffinet, C.; Kulik, H. J. New Strategies for Direct Methane-to-Methanol Conversion from Active Learning Exploration of 16 Million Catalysts. *JACS Au* **2022**, *2*, 1200−1213.
(57) Liu, M. J.; Nazemi, A.; Taylor, M. G.; Nandy, A.; Duan, C. R.; Steeves, A. H.; Kulik, H. J. Large-Scale Screening Reveals That Geometric Structure Matters More Than Electronic Structure in the Bioinspired Catalyst Design of Formate Dehydrogenase Mimics. *ACS Catal.* **2022**, *12*, 383−396.
(58) Beyer, M. K. The Mechanical Strength of a Covalent Bond Calculated by Density Functional Theory. *J. Chem. Phys.* **2000**, *112*, 7307−7312.
(59) Wang, J. P.; Kouznetsova, T. B.; Kean, Z. S.; Fan, L.; Mar, B. D.; Martínez, T. J.; Craig, S. L. A Remote Stereochemical Lever Arm Effect in Polymer Mechanochemistry. *J. Am. Chem. Soc.* **2014**, *136*, 15162−15165.
(60) Klein, I. M.; Husic, C. C.; Kovacs, D. P.; Choquette, N. J.; Robb, M. J. Validation of the CoGEF Method as a Predictive Tool for Polymer Mechanochemistry. *J. Am. Chem. Soc.* **2020**, *142*, 16364−16381.
(61) Kevlishvili, I.; Vakil, J.; et al. High-Throughput Discovery of Ferrocene Mechanophores with Enhanced Reactivity and Network Toughening. *ChemRxiv* **2024**, DOI: 10.26434/chemrxiv-2024-dsj2g.
(62) Kulik, H. J. Modeling Mechanochemistry from First Principles. *Rev. Comp Ch* **2018**, *31*, 265−311.
(63) Ong, M. T.; Leiding, J.; Tao, H.; Virshup, A. M.; Martínez, T. J. First Principles Dynamics and Minimum Energy Pathways for Mechanochemical Ring Opening of Cyclobutene. *J. Am. Chem. Soc.* **2009**, *131*, 6377.
(64) Chen, Z.; Zhu, X.; Yang, J.; Mercer, J. A. M.; Burns, N. Z.; Martinez, T. J.; Xia, Y. The Cascade Unzipping of Ladderane Reveals Dynamic Effects in Mechanochemistry. *Nat. Chem.* **2020**, *12*, 302−309.
(65) Mar, B. D.; Qi, H. W.; Liu, F.; Kulik, H. J. Ab Initio Screening Approach for the Discovery of Lignin Polymer Breaking Pathways. *J. Phys. Chem. A* **2015**, *119*, 6551−6562.
(66) Mar, B. D.; Kulik, H. J. Depolymerization Pathways for Branching Lignin Spirodienone Units Revealed with Ab Initio Steered Molecular Dynamics. *J. Phys. Chem. A* **2017**, *121*, 532−543.
(67) Ribas-Arino, J.; Shiga, M.; Marx, D. Understanding Covalent Mechanochemistry. *Angew. Chem. Int. Edit* **2009**, *48*, 4190−4193.
(68) Dopieralski, P.; Ribas-Arino, J.; Marx, D. Force-Transformed Free-Energy Surfaces and Trajectory-Shooting Simulations Reveal the Mechano-Stereochemistry of Cyclopropane Ring-Opening Reactions. *Angew. Chem. Int. Edit* **2011**, *50*, 7105−7108.
(69) Dopieralski, P.; Ribas-Arino, J.; Anjukandi, P.; Krupicka, M.; Marx, D. Unexpected Mechanochemical Complexity in the Mechanistic Scenarios of Disulfide Bond Reduction in Alkaline Solution. *Nat. Chem.* **2017**, *9*, 164−170.
(70) Nixon, R.; De Bo, G. Isotope Effect in the Activation of a Mechanophore. *J. Am. Chem. Soc.* **2021**, *143*, 3033−3036.
(71) Sun, Y.; Kevlishvili, I.; Kouznetsova, T. B.; Burke, Z. P.; Craig, S. L.; Kulik, H. J.; Moore, J. S. The Tension-Activated Carbon−Carbon Bond. *Chem.* **2024**, *10*3055.
(72) Wilbraham, L.; Adamo, C.; Ciofini, I. Communication: Evaluating Non-Empirical Double Hybrid Functionals for Spin-State Energetics in Transition-Metal Complexes. *J. Chem. Phys.* **2018**, *148*, No. 041103.
(73) Finney, B. A.; Chowdhury, S. R.; Kirkvold, C.; Vlaisavljevich, B. CASPT2 Molecular Geometries of Fe(II) Spin-Crossover Complexes. *Phys. Chem. Chem. Phys.* **2022**, *24*, 1390−1398.
(74) Roy Chowdhury, S.; Nguyen, N.; Vlaisavljevich, B. Importance of Dispersion in the Molecular Geometries of Mn(III) Spin-Crossover Complexes. *J. Phys. Chem. A* **2023**, *127*, 3072−3081.
(75) Phung, Q. M.; Feldt, M.; Harvey, J. N.; Pierloot, K. Toward Highly Accurate Spin State Energetics in First-Row Transition Metal Complexes: A Combined CASPT2/CC Approach. *J. Chem. Theory Comput* **2018**, *14*, 2446−2455.
(76) Phung, Q. M.; Martin-Fernandez, C.; Harvey, J. N.; Feldt, M. Ab Initio Calculations for Spin-Gaps of Non-Heme Iron Complexes. *J. Chem. Theory Comput* **2019**, *15*, 4297−4304.
(77) Li Manni, G.; Carlson, R. K.; Luo, S. J.; Ma, D. X.; Olsen, J.; Truhlar, D. G.; Gagliardi, L. Multiconfiguration Pair-Density Functional Theory. *J. Chem. Theory Comput* **2014**, *10*, 3669−3680.
(78) Wilbraham, L.; Verma, P.; Truhlar, D. G.; Gagliardi, L.; Ciofini, I. Multiconfiguration Pair-Density Functional Theory Predicts Spin State Ordering in Iron Complexes with the Same Accuracy as Complete Active Space Second-Order Perturbation Theory at a

Significantly Reduced Computational Cost. *J. Phys. Chem. Lett.* **2017**, *8*, 2026−2030.
(79) Reiher, M.; Salomon, O.; Artur Hess, B. Reparameterization of Hybrid Functionals Based on Energy Differences of States of Different Multiplicity. *Theor. Chem. Acc.* **2001**, *107*, 48−55.
(80) Radon, M. Revisiting the Role of Exact Exchange in DFT Spin-State Energetics of Transition Metal Complexes. *Phys. Chem. Chem. Phys.* **2014**, *16*, 14479−14488.
(81) Ioannidis, E. I.; Kulik, H. J. Towards Quantifying the Role of Exact Exchange in Predictions of Transition Metal Complex Properties. *J. Chem. Phys.* **2015**, *143*, No. 034104.
(82) Gani, T. Z. H.; Kulik, H. J. Unifying Exchange Sensitivity in Transition-Metal Spin-State Ordering and Catalysis through Bond Valence Metrics. *J. Chem. Theory Comput* **2017**, *13*, 5443−5457.
(83) Ye, S. F.; Neese, F. Accurate Modeling of Spin-State Energetics in Spin-Crossover Systems with Modern Density Functional Theory. *Inorg. Chem.* **2010**, *49*, 772−774.
(84) Vennelakanti, V.; Taylor, M. G.; Nandy, A.; Duan, C.; Kulik, H. J. Assessing the Performance of Approximate Density Functional Theory on 95 Experimentally Characterized Fe(II) Spin Crossover Complexes. *J. Chem. Phys.* **2023**, *159*, No. 024120.
(85) Duan, C. R.; Chen, S. X.; Taylor, M. G.; Liu, F.; Kulik, H. J. Machine Learning to Tame Divergent Density Functional Approximations: A New Path to Consensus Materials Design Principles. *Chem. Sci.* **2021**, *12*, 13021−13036.
(86) Nance, J.; Bowman, D. N.; Mukherjee, S.; Kelley, C. T.; Jakubikova, E. Insights into the Spin-State Transitions in [Fe(Tpy)]: Importance of the Terpyridine Rocking Motion. *Inorg. Chem.* **2015**, *54*, 11259−11268.
(87) Bowman, D. N.; Jakubikova, E. Low-Spin Versus High-Spin Ground State in Pseudo-Octahedral Iron Complexes. *Inorg. Chem.* **2012**, *51*, 6011−6019.
(88) Groom, C. R.; Bruno, I. J.; Lightfoot, M. P.; Ward, S. C. The Cambridge Structural Database. *Acta Crystallographica Section B* **2016**, *72*, 171−179.
(89) Gütlich, P.; Goodwin, H. A. Spin Crossover: An Overall Perspective. *Top Curr. Chem.* **2004**, *233*, 1−47.
(90) Goodwin, H. A. Spin Crossover in Iron(II) Tris(Diimine) and Bis(Terimine) Systems. *Top Curr. Chem.* **2004**, *233*, 59−90.
(91) Goodwin, H. A. Spin Crossover in Cobalt(II) Systems. *Spin Crossover in Transition Metal Compounds Ii* **2004**, *234*, 23−47.
(92) Kumar, K. S.; Ruben, M. Sublimable Spin-Crossover Complexes: From Spin-State Switching to Molecular Devices. *Angew. Chem. Int. Edit* **2021**, *60*, 7502−7521.
(93) Stevenson, R.; De Bo, G. Controlling Reactivity by Geometry in Retro-Diels-Alder Reactions under Tension. *J. Am. Chem. Soc.* **2017**, *139*, 16768−16771.
(94) Qian, H.; Purwanto, N. S.; Ivanoff, D. G.; Halmes, A. J.; Sottos, N. R.; Moore, J. S. Fast, Reversible Mechanochromism of Regioisomeric Oxazine Mechanophores: Developing Responsive Force Probes for Polymeric Materials. *Chem.* **2021**, *7*, 1080−1091.
(95) Lin, Y. J.; Barbee, M. H.; Chang, C. C.; Craig, S. L. Regiochemical Effects on Mechanophore Activation in Bulk Materials. *J. Am. Chem. Soc.* **2018**, *140*, 15969−15975.
(96) Kumpfer, J. R.; Rowan, S. J. Thermo-, Photo-, and Chemo-Responsive Shape-Memory Properties from Photo-Cross-Linked Metallo-Supramolecular Polymers. *J. Am. Chem. Soc.* **2011**, *133*, 12866−12874.
(97) Neese, F.; Wennmohs, F.; Becker, U.; Riplinger, C. The Orca Quantum Chemistry Program Package. *J. Chem. Phys.* **2020**, *152*, No. 224108.
(98) Neese, F. Software Update: The Orca Program System-Version 5.0. *Wires Comput. Mol. Sci.* **2022**, *12*, No. e1606.
(99) Weigend, F.; Ahlrichs, R. Balanced Basis Sets of Split Valence, Triple Zeta Valence and Quadruple Zeta Valence Quality for H to Rn: Design and Assessment of Accuracy. *Phys. Chem. Chem. Phys.* **2005**, *7*, 3297−305.
(100) Becke, A. D. Density-Functional Thermochemistry. III. The Role of Exact Exchange. *J. Chem. Phys.* **1993**, *98*, 5648−5652.
(101) Lee, C.; Yang, W.; Parr, R. G. Development of the Colle-Salvetti Correlation-Energy Formula into a Functional of the Electron Density. *Phys. Rev. B* **1988**, *37*, 785−789.
(102) Stephens, P. J.; Devlin, F. J.; Chabalowski, C. F.; Frisch, M. J. Ab Initio Calculation of Vibrational Absorption and Circular Dichroism Spectra Using Density Functional Force Fields. *J. Phys. Chem.* **1994**, *98*, 11623−11627.
(103) Grimme, S.; Antony, J.; Ehrlich, S.; Krieg, H. A Consistent and Accurate Ab Initio Parametrization of Density Functional Dispersion Correction (DFT-D) for the 94 Elements H-Pu. *J. Chem. Phys.* **2010**, *132*, No. 154104.
(104) Becke, A. D.; Johnson, E. R. A Density-Functional Model of the Dispersion Interaction. *J. Chem. Phys.* **2005**, *123*, No. 154101.
(105) Eckert, F.; Pulay, P.; Werner, H. J. Ab Initio Geometry Optimization for Large Molecules. *J. Comput. Chem.* **1997**, *18*, 1473−1483.
(106) Ioannidis, E. I.; Gani, T. Z. H.; Kulik, H. J. Molsimplify: A Toolkit for Automating Discovery in Inorganic Chemistry. *J. Comput. Chem.* **2016**, *37*, 2106−2117.
(107) Bhandary, S.; Tomczak, J. M.; Valli, A. Designing a Mechanically Driven Spin-Crossover Molecular Switch Organic Embedding. *Nanoscale Adv.* **2021**, *3*, 4990−4995.
(108) Garcia, Y.; Gütlich, P. Thermal Spin Crossover in Mn(II), Mn(III), Cr(II) and Co(III) Coordination Compounds. *Spin Crossover in Transition Metal Compounds II* **2004**, *234*, 49−62.
(109) Pedregosa, F.; Varoquaux, G.; Gramfort, A.; Michel, V.; Thirion, B.; Grisel, O.; Blondel, M.; Prettenhofer, P.; Weiss, R.; Dubourg, V.; et al. Scikit-Learn: Machine Learning in Python. *J. Mach Learn Res.* **2011**, *12*, 2825−2830.
(110) Bühl, M.; Reimann, C.; Pantazis, D. A.; Bredow, T.; Neese, F. Geometries of Third-Row Transition-Metal Complexes from Density-Functional Theory. *J. Chem. Theory Comput* **2008**, *4*, 1449−1459.
(111) Jensen, K. P.; Roos, B. O.; Ryde, U. Performance of Density Functionals for First Row Transition Metal Systems. *J. Chem. Phys.* **2007**, *126*, No. 014103.
(112) Beech, H. K.; Wang, S.; Sen, D.; Rota, D.; Kouznetsova, T. B.; Arora, A.; Rubinstein, M.; Craig, S. L.; Olsen, B. D. Reactivity-Guided Depercolation Processes Determine Fracture Behavior in End-Linked Polymer Networks. *ACS Macro Lett.* **2023**, *12*, 1685−1691.
(113) Tennyson, A. G.; Wiggins, K. M.; Bielawski, C. W. Mechanical Activation of Catalysts for C-C Bond Forming and Anionic Polymerization Reactions from a Single Macromolecular Reagent (Vol 132, Pg 16631, 2010). *J. Am. Chem. Soc.* **2015**, *137*, 3429−3429.
(114) Huang, X.; Kevlishvili, I.; Craig, S. L.; Kulik, H. J. Zenodo Repository for Force-Activated Spin-Crossover in Fe2+ and Co2+ Transition Metal Mechanophores. 2024. . (Accessed 10/23/24).

https://doi.org/10.1021/acs.inorgchem.4c04732
Inorg. Chem. 2025, 64, 380−392